The Journal of Infectious Diseases

SUPPLEMENT ARTICLE

The Use of Large-Particle Aerosol Exposure to Nipah Virus to Mimic Human Neurological Disease Manifestations in the African Green Monkey

Ji Hyun Lee,[1] Dima A. Hammoud,[2] Yu Cong,[1] Louis M. Huzella,[1] Marcelo A. Castro,[1] Jeffrey Solomon,[3] Joseph Laux,[1] Matthew Lackemeyer,[1] J. Kyle Bohannon,[1] Oscar Rojas,[1] Russ Byrum,[1] Ricky Adams,[1] Danny Ragland,[1] Marisa St Claire,[1] Vincent Munster,[4] and Michael R. Holbrook[1]

[1]National Institute of Allergy and Infectious Diseases, Integrated Research Facility, Ft Detrick, Frederick, Maryland, USA, [2]Center for Infectious Disease Imaging, National Institutes of Health, Clinical Center, Bethesda, Maryland, USA, [3]Clinical Monitoring Research Program Directorate, Frederick National Laboratory for Cancer Research sponsored by the National Cancer Institute, Frederick, Maryland, USA, [4]Virus Ecology Unit, Laboratory of Virology, Rocky Mountain Laboratories, Hamilton, Montana, USA

Nipah virus (NiV) is an emerging virus associated with outbreaks of acute respiratory disease and encephalitis. To develop a neurological model for NiV infection, we exposed 6 adult African green monkeys to a large-particle (approximately 12 μm) aerosol containing NiV (Malaysian isolate). Brain magnetic resonance images were obtained at baseline, every 3 days after exposure for 2 weeks, and then weekly until week 8 after exposure. Four of six animals showed abnormalities reminiscent of human disease in brain magnetic resonance images. Abnormalities ranged from cytotoxic edema to vasogenic edema. The majority of lesions were small infarcts, and a few showed inflammatory or encephalitic changes. Resolution or decreased size in some lesions resembled findings reported in patients with NiV infection. Histological lesions in the brain included multifocal areas of encephalomalacia, corresponding to known ischemic foci. In other regions of the brain there was evidence of vasculitis, with perivascular infiltrates of inflammatory cells and rare intravascular fibrin thrombi. This animal model will help us better understand the acute neurological features of NiV infection and develop therapeutic approaches for managing disease caused by NiV infection.

Keywords. Nipah virus; Paramyxovirus; Magnetic resonance imaging; Computed tomography; pathology.

Nipah virus (NiV), a highly pathogenic paramyxovirus (genus *Henipavirus*), is an emerging pathogen associated with outbreaks of acute respiratory and neurological disease. The first recognized outbreaks of NiV encephalitis primarily affected pig farmers in Malaysia and Singapore from 1998 to 1999, resulting in 265 human cases with 105 deaths [1–4]. NiV infection reemerged in 2001, resulting in >54 deaths in Bangladesh and India [5]. NiV is transmitted to humans through contact with excreta of *Pteropus* spp. bats or with pigs, and through human-to-human contact, including nosocomial infections [6, 7]. NiV infection in humans can cause an acute febrile disease with development of atypical pneumonia, an acute respiratory distress syndrome (ARDS)–like disease [8], and neurological disease; in some cases, the only manifestations are neurological [9–11]. Symptoms of NiV infection include cough, respiratory distress, fever, headache, drowsiness, seizures, areflexia, hypertension, and vomiting [9, 10]. Many survivors of NiV infection experience long-term neurological sequelae including myoclonus, personality changes, cognitive impairment or depression, and persistent abnormalities on brain magnetic resonance (MR) images [12, 13].

Brain MR imaging of individuals with neurological symptoms from Malaysia and Singapore showed white matter lesions, both subcortical and periventricular, on T2-weighted fluid-attenuated inversion-recovery (FLAIR) images. Some of the lesions were associated with restricted diffusion consistent with ischemia [14–16]. Some reports described resolution or reduction of these lesions, whereas others described eventual appearance of high signal intensity foci on T1-weighted images [15, 16]. Long-term neurological manifestations of the infection, on the other hand, manifested as confluent cortical and subcortical signal abnormalities and cortical atrophy [13]. Chest radiographs of infected individuals in a Bangladesh NiV outbreak showed diffuse bilateral opacities consistent with ARDS [8], which suggest edema, interstitial thickening, or inflammation in the lung parenchyma [17]. The Case fatality rates of NiV infection occurring in outbreaks in Bangladesh from 2001–2019 are about 70% [18].

Currently no therapies or vaccines are approved for NiV infection in humans or livestock species. To develop effective therapeutics for NiV infection, it is essential to identify and characterize animal models that mimic the various aspects of human disease. To this end, we evaluated NiV infection in African green monkeys (AGMs) using a large-particle aerosol containing the Malaysian strain of NiV to study the

Presented in part: International Society for Magnetic Resonance Imaging 2019 Annual Meeting 2019.

Correspondence: Michael R. Holbrook, National Institute of Allergy and Infectious Diseases Integrated Research Facility, 8200 Research Plaza, Ft Detrick, Frederick, MD, 21702 (Michael.holbrook@nih.gov).

The Journal of Infectious Diseases® 2020;221(S4):S419–30

Published by Oxford University Press for the Infectious Diseases Society of America 2019. This work is written by (a) US Government employee(s) and is in the public domain in the US.

DOI: 10.1093/infdis/jiz502

neuropathogenic properties of NiV. This novel approach was designed to ensure deposition of the virus in the nasopharynx and nasal cavity. The approximation of particle deposition is based on previous work demonstrating the deposition pattern of fluorine-18 fluorodeoxyglucose-laden aerosols in non-human primates using positron emission tomography or computed tomography (CT) [19].

NiV disease has previously been investigated in the AGM model after intratracheal [20–23], intraperitoneal [24], or small-particle (<3 μm) [23] and medium-particle (approximately 7 μm) [25] aerosol exposure. These studies identified aspects of infection that are similar to human NiV disease, but model only certain aspects of it. Previous studies also demonstrated that aerosol exposure to medium-sized particles (approximately 7 μm) at a lower challenge dose (approximately 100 plaque-forming units [PFUs]) extended the disease course (12.5 days after exposure) relative to intratracheal or small-particle aerosol inoculation (8 days after exposure) and resulted in brain lesions in some animals, detected with MR imaging [23, 25]. Typical lesions noted in the brains of AGMs experimentally infected with NiV consisted of ischemia-induced encephalomalacia and lymphohistiocytic, often perivascular inflammation, with some hemorrhage and fibrin deposition [20]. Therefore, a lower aerosol dose targeting the upper respiratory tract is most likely the inoculation route required to achieve the goals of extending the disease course and studying neurological disease.

In the current study, our objective was to develop a consistent animal model for neurological NiV infection that more closely mimics a potential and realistic exposure route for humans. We evaluated the pathological response in animals subjected to a low dose of virus inoculum (approximately 500 PFUs) in a large-particle aerosol exposure to ensure deposition of NiV in the nasopharynx and nasal cavity. Using brain MR imaging, we assessed the NiV-infected AGMs for similarities to reported imaging findings in NiV-infected humans. We also performed cage-side observations to identify overt neurological signs of disease and histopathological studies to determine the nature of identified lesions.

METHODS

Ethics Statement

Work with non-human primates was conducted in accordance with an animal study protocol approved by the National Institute of Allergy and Infectious Diseases (NIAID), Division of Clinical Research, Animal Care and Use Committee following recommendations in the *Guide for the Care and Use of Laboratory Animals* [26]. This institution also accepts as mandatory the Public Health Service policy on the humane care and use of laboratory animals (https://olaw.nih.gov/policies-laws/phs-policy.htm). All animal work at NIAID was performed in a facility accredited by the Association for the Assessment and Accreditation of Laboratory Animal Care International. All work with non-human primates was done in accordance with the recommendations of the Weatherall Report.

Virus and Cells

The Malaysian isolate of NiV (NiV-M) used in this study was isolated from a fatal human case in 1998 [1], as described elsewhere [25]. The virus was passaged 6 times in Vero-E6 or Vero cells, and the stock virus sequence information was submitted to GenBank (accession no. KY425646.1) All work with viable NiV was performed in the biosafety level 4 (BSL-4) facility at the NIAID Integrated Research Facility in Frederick, Maryland.

Animals

Wild-caught Caribbean origin AGMs were purchased from PrimGen. Six adult AGMs (3 male and 3 female; 3–7 kg) prescreened for NiV antibodies by means of neutralization assay or enzyme-linked immunosorbent assay were divided into 2 groups to accommodate imaging time and logistics. Animal housing, enrichment, and general protocol for anesthetizing animals are described elsewhere [23, 25].

Study Design

The study animals were exposed to a large-particle aerosol challenge at the target dose of approximately 500 PFUs (confirmed by back-titration) of NiV-M on day 0. Physical examinations and blood collection were performed on days −62, −20, 3, 6, 9, 12, 15, 21, 28, 35, 42, and 49, and at euthanasia. After infection, all animals were monitored daily and anesthetized on days after exposure listed above or before unscheduled euthanasia, for physical examinations, for collection of samples, including blood and swab (nasal and oral) samples, and for whole-body CT and brain MR imaging with and without contrast agent to examine brain morphological changes. Cerebrospinal fluid (CSF) samples were collected weekly from surviving animals beginning on or about day 21 after exposure to NiV until study termination. The animals were observed at least twice daily for clinical signs of disease, according to the Animal Care and Use Committee–approved end-point criteria.

Aerosol Exposure

Six AGMs were exposed to a target dose of approximately 500 PFUs in a large-particle aerosol challenge with an NiV-M isolate using a 16.0-L, head-only aerosol exposure chamber. An aerosol management platform (AeroMP; Biaera Technologies) within a class III biosafety cabinet (Germfree) was used to conduct the aerosol challenge. The animals were anesthetized with ketamine (10.0 mg/kg, intramuscular) and tiletamine and zolazepam (3.0–6.0 mg/kg, intramuscular) and received a single, time-calculated aerosol challenge dose [27]. The average particle size ranged from 11.0 to 12.5 μm, targeting the extrathoracic or nasopharyngeal region of the respiratory tract. An air wash period of 5 minutes between each aerosol challenge run allowed the previously generated particles within the exposure chamber to

decay. The presented dose was calculated based on the back-titration of samples collected from the aerosol chamber [25].

Clinical Pathology

Clinical chemistry analyses were performed on a Piccolo chemistry analyzer (Abaxis) using the General Chemistry panel. Complete blood counts were determined using a Sysmex XT2000*i*V analyzer (Sysmex). Data were graphed using Prism software (GraphPad versions 7 and 8).

Viral Loads

Whole blood, serum, swab, and brain cerebral tissue samples (≥200 mg each for brain tissue samples, including gray matter, white matter, and ventricles with and without lesions) were collected and inactivated in TRIzol LS (Invitrogen) at necropsy. Total RNA was isolated using the QIAamp Viral RNA Mini Kit (GSS Qiagen). Briefly, 70 µL of TRIzol LS-inactivated sample was added to 280 µL of Qiagen Buffer AVL containing carrier RNA. The sample was eluted in 70 µL of Qiagen Buffer AVE, aliquoted, and frozen until assayed. Then viral loads of the sample were measured using an in-house validated quantitative reverse-transcription polymerase chain reaction assay for NiV and reported as viral RNA copies ($\log_{10}$) per milliliter of sample versus days after exposure [28]. In each run, standards and controls were verified to have met all acceptance criteria. The standard curve executed for this assay was from 1×10^9 (upper limit of quantification) through 1×10^2 (lower limit of quantification).

Imaging

High-resolution whole-body CT scans of the AGMs were acquired in the transaxial plane with free breathing and with the following parameter settings: 140 kVp, 300 mAs per section, 1-mm thickness, 0.5-mm increments, 0.438-mm pitch, 16 × 0.75 collimation, and 0.5-second rotation. Images were reconstructed in a pixel size of 0.49 mm with a 250-mm field of view, and with the section spacing changed to 0.5 mm.

On transport to the MR imaging room, animals were prepped with an intravenous catheter in an arm vein before entering the imaging suite, and a line prefilled with gadobutrol was used for manual injection, followed by a saline bolus to flush the system. Structural, quantitative, and functional brain MR images were obtained using with a pediatric head/supine coil (head element section with 4 channels). All sections were acquired in the transaxial plane.

A series of imaging sequences was obtained to examine the brain for indications of inflammation or lesions due to NiV infection. These sequences included T2-weighted turbo spin-echo and T1-weighted fast-field-echo (FFE), diffusion tensor (DT), and T2-weighted FLAIR sequences. The FLAIR and T1-weighted FFE images were obtained both before and after contrast enhancement. T1 maps were computed using a dual flip angle method from T1-weighted FFE images [29]. Diffusion-weighted (DW) images, trace of the DT (trace [DT]), and fractional anisotropy maps were created from DT images [30–32]. The combination of these MR imaging sequences typically identifies cytotoxic and vasogenic edema as hyperintense regions on T2-weighted and FLAIR images; changes in the diffusion patterns, such as restricted diffusion, indicated by hypointense signal in trace (DT) maps computed from DT images; and blood-brain barrier disruption by comparing T1 maps computed from T1-weighted FFE images before and after contrast injection. All images were reviewed by 2 radiologists.

Image Analysis

Each lesion with hypersignal intensity of FLAIR/T2 and/or abnormal diffusivity was first segmented, and the volume contour was mirrored onto the intact brain for comparison using MIM software (MIM Software version 6.9). The volumes of interest were then retrospectively projected on previous images and onto different sequences after rigid registration. Changes in trace (DT) values were measured.

Brain parenchymal volumes were estimated from synthetic T1-weighted MR images by combining the gray and white matter volumes. First, the brain MR images were coregistered to a rhesus macaque template brain using deformable transformation [33]. A deskulled version of this coregistered template brain allowed for brain deskulling (removal of all tissue outside of the brain) from the synthetic T1W image. Then the deskulled brain was segmented into gray matter, white matter, and CSF using a fuzzy c-means clustering algorithm that incorporates anisotropic diffusion filtering and bias-correction as preprocessing steps. Total brain volume was measured.

Necropsy and Histopathology

Tissue samples collected at necropsy were fixed for 72 hours in 10% neutral buffered formalin. After fixation and removal from the BSL-4 laboratory, tissue samples were processed in a Tissue-Tek VIP-6 automated vacuum infiltration processor (Sakura Finetek USA), followed by paraffin embedding with a Tissue-Tek model TEC unit (Sakura Finetek USA). Using a standard semiautomated rotary microtome and lighted water flotation bath (Leica Biosystems), tissue sections were cut to a thickness of 4 µm and mounted on positively charged uncoated glass slides (ThermoFisher), air dried at room temperature, stained with hematoxylin-eosin, and covered with a cover slip for microscopic evaluation by the pathologist.

Immunohistochemistry

Immunohistochemistry was performed on the tissue of interest using commercial antibodies against CD3G (rabbit polyclonal anti-CD3G; EPR4517), CD68 (Novus mouse monoclonal anti-CD68), glial fibrillary acidic protein (GFAP) (rabbit polyclonal anti-GFAP [Dako]), ionized calcium-binding adaptor molecular 1 (Iba1) (goat polyclonal anti-Iba1), and neuronal nuclei (NeuN) (rabbit polyclonal anti-NeuN). A non-commercial

antibody was used for NiV: rabbit polyclonal anti-NIPAH (IRF reference# sGNIV PA8905 D70,72).

RESULTS

Clinical Presentation

Six AGMs were exposed to NiV-M by large-particle aerosol. The measured particle size for these exposures ranged from 11.0 to 12.5 μm. The calculated exposure dose based on back-titration was 224.4–773.7 PFUs (Table 1). In all graphs, the black lines represent NiV survivors, and the gray lines, animals that did not survive infection. After exposure, only mild weight loss in all the animals (mean [standard deviation], 4.5% [3.6%]) (Supplementary Figure 1*A*) was observed despite reduced appetite and marked dehydration at necropsy. One of the 6 animals (8212) remained completely asymptomatic without evidence of infection through the study end point. A second animal (8671) with evidence of infection (Table 1) became feverish on day 6 after exposure (Supplementary Figure 1*B*) and became inappetent and mildly anemic from day 6 through day 22 after exposure (mean hemoglobin level, 11.4 mg/dL [12% below baseline]; mean hematocrit, 38.0% [9% below baseline]) (Supplementary Figure 2), but this animal recovered and was clinically normal at the study end point [34].

The 4 remaining study animals (8168, 8112, 8078, and 8233) became clinically ill, achieved progressive clinical scores, and were euthanized in extremis on days 5, 16, 17, and 20 after exposure (Figure 1*A*). Their average postexposure survival time was approximately 14.5 days. No clear relationship was found between the dose received and survival time (data not shown). In 1 of the 4 clinically ill animals (8168), an acute respiratory syndrome suggestive of ARDS developed (Supplementary Figure 3), with fever (Supplementary Figure 1B), increased respiration rate, dehydration, and depression; this animal was euthanized on day 5 after exposure.

In the 3 remaining animals (8112, 8078, and 8233), a clinical syndrome developed that was characterized by generalized progressive weakness, nonresponsiveness, and depression; these animals died on days 16, 17, and 20 after exposure (Figure 1*A*), respectively. All 3 exhibited neurological signs consisting of intention tremors, eyelid twitching, and generalized shaking. The prodromal period for the 3 affected animals was prolonged, with no abnormal clinical observations until day 6 after exposure, when they became anorectic and their body temperatures (mean at baselike = 37.4°C) began to increase, reaching a mean of 39.4°C ℃ on day 15 after exposure (Supplementary Figure 1*B*).

The clinical disease in 2 affected animals (8078 and 8233) progressed identically from day 3 after exposure until they became moribund and were euthanized. At their study end points, both animals had a mild, progressive, relative, anemia (mean hematocrit, 39.8%, or 15% below baseline; mean hemoglobin level, 12.6 mg/dL, or 16% below baseline; mean red blood cell count, 5.29 million/dL, or 17.3% below baseline) (Supplementary Figure 2), whereas the third animal (8112) maintained normal erythrocyte indices through the study end point. All 3 animals revealed a similar pattern of platelet reduction beginning on day 3 after exposure, from a mean baseline of 319 000/dL, dipping as low as 113 000/dL on day 15 after exposure, a 64.6% loss. Two of the 3 animals had severe thrombocytopenia at their study end points. All 3 animals were severely dehydrated at necropsy, which probably masked a more severe anemia and thrombocytopenia than laboratory results indicated. From the serum chemistry profile, only calcium, albumin, and total protein became mildly reduced and failed to normalize through the study end point (Supplementary Figure 4).

Viral Dissemination

Viral genomic RNA concentrations were determined in whole blood, serum, CSF, and oral nasal swab samples over the course of disease and at necropsy. Viral RNA concentrations of 3–6 $\log_{10}$/mL were detected in whole blood samples at 12 days after exposure in 1 animal (8112) and at day 15 after exposure in other 2 animals (8078 and 8233) (Figure 1*B*). The profile in serum was similar to that whole blood in most animals except 8233 (Figure 1*B* and 1*C*). In the CSF, only 2 animals (8078 and 8112) showed a viral load at necropsy (Figure 1*D*). Peak viral genome concentrations were detected in oral and nasal mucosa from one of the survivors (8671) 9 days after exposure, and returned to normal by 12 days after exposure (Figure 1*E* and 1*F*).

To demonstrate the presence of NiV RNA in selected tissues collected at necropsy, viral genomic RNA was quantified. Viral RNA was measured from peripheral tissues and brain cerebrum at variable locations with or without lesions. Viral RNA concentrations of >3 to <7 $\log_{10}$ genome copies/mg of tissue were detected in animals that succumbed to the infection (8078, 8112, and 8233) in samples from different parts of the brain with or without lesions (Supplementary Figure 5). Viral RNA was detected in animal 8112 in parts of the brain that did not contain lesions, but not in tissues from the same brain regions that contained a lesion.

Brain MR Imaging

Routine brain MR imaging of animals involved in this study found that 4 of 6 animals (66.7%) showed abnormalities reminiscent of human NiV-induced disease in MR imaging, including in 1 animal that survived the infection. In the first animal (8078), FLAIR imaging first showed a small focus of restricted diffusion in the left frontal subcortical white matter on day 15 after exposure (Figure 2*A*). Multiple bilateral cerebral lesions with similar characteristics became apparent on day 17 after exposure on T2-weighted images (terminal day; Figure 2*B*). Increased signal intensity highlighted 6 of 7 lesions on T2-weighted, FLAIR, and DW images, with decreased

Table 1. Summary of Clinical and Serial Magnetic Resonance Imaging Findings in African Green Monkeys Infected With Nipah Virus

			Acute Infection		Findings After 1 mo				
Animal ID /Sex/ Terminal Day	NiV-M Dose, PFUs	Particle Size, μm	Lesions, No./Location on MR Images	Restricted/Nonrestricted Lesions on DW MR Images, No./Trace (DT)	Lesions on FLAIR Images, No.	Lesions on T1-Weighted Images, No.	Lesions on DT/FA Images, No.	Clinical Status at Euthanasia	Terminal Weight, kg/ Averaged Preexposed Weight, kg (change, %)
8078 /M/17	773.7	12.5	7/Left frontal white matter, bilateral cerebral lesions, left internal capsule, brainstem	6/1/1440/2191	NP	NP	NP	Weakness; nonresponsiveness	6.00/6.34 (–5.4)
8112 /F/16	519.7	11.5	1/Right internal capsule/lateral thalamus	1/0/1563/	NP	NP	NP	Weakness; tremors; nonresponsiveness	4.38/4.57 (–4.2)
8212 /M/63	510	12.7	0	0	0	0	0	Survivor; normal	5.74/6.21 (–7.6)
8168/M/5[a]	347.7	11.1	0	0	NP	NP	NP	Depression; dehydration; nonresponsiveness; rapid respiration; SpO_2, 83%	6.78/6.80 (–0.3)
8233 /F/20	326.6	11	5/Pons, brainstem, right frontal white matter, left olfactory lobe	0/5/NA/2251	NP	NP	NP	Weakness; nonresponsiveness; depression; tremors; ear twitch	4.00/4.40 (–9.1)
8671 /F/56	224.4	11.4	2/Left cerebellar hemisphere, right frontal white matter	0/2/NA/2897	1	1	1	Survivor; normal	3.56/3.58 (–0.6)

Abbreviations: DT, diffusion tensor; DW, diffusion-weighted; FA, fractional anisotropy; FLAIR, fluid-attenuated inversion-recovery; ID, identifier; MR, magnetic resonance; NA, not available; NiV-M, Nipah virus Malaysian isolate; NP, not performed; PFUs, plaque-forming units; trace (DT), trace of diffusion tensor; SpO_2, peripheral oxygen saturation.

[a]Animal 8168 was euthanized on day 5 after infection with an acute respiratory syndrome. No measurable viral load.

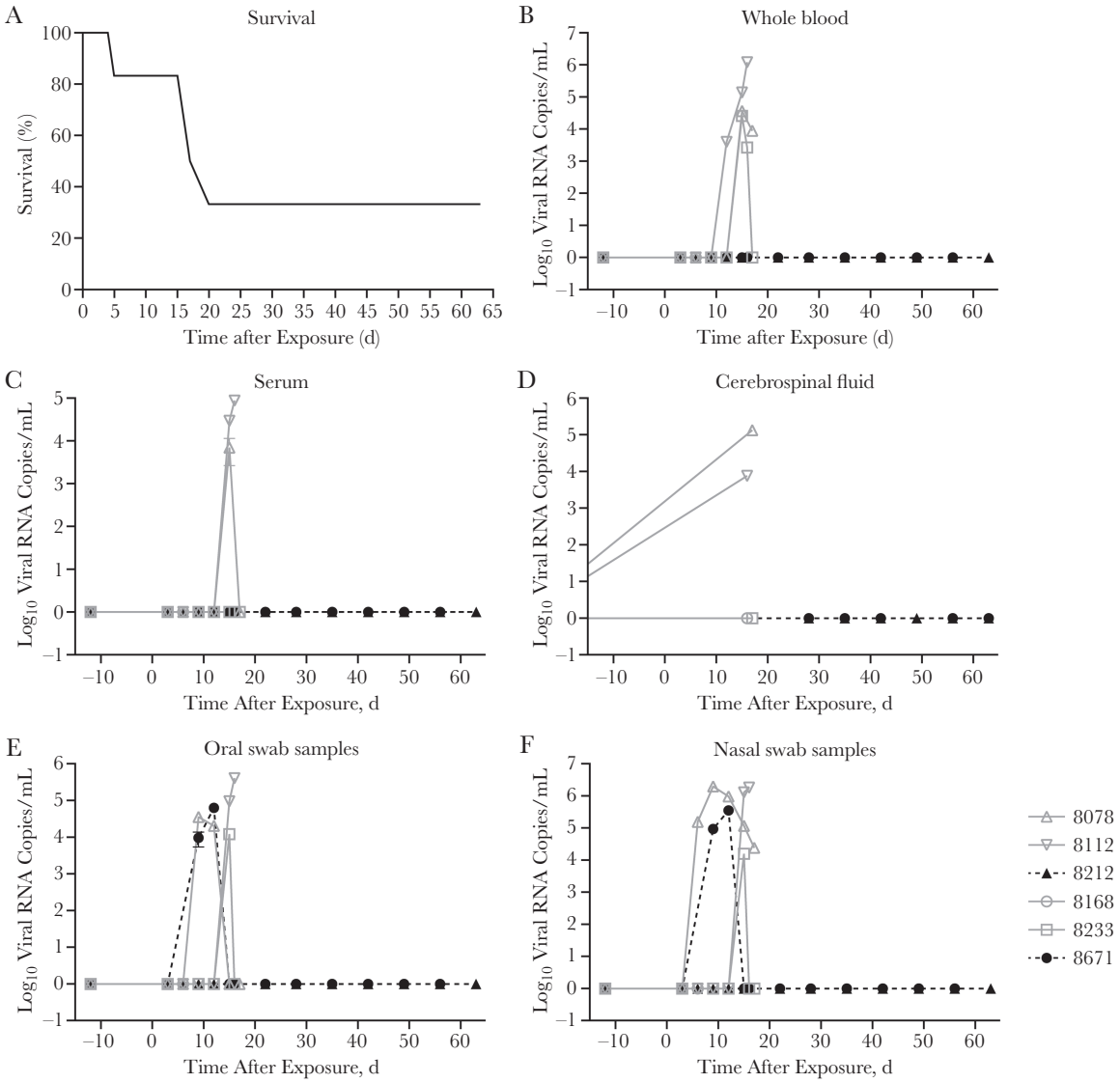

Figure 1. Incidence of survival in African green monkeys after Nipah virus (NiV) challenge and resulting viremia and cerebrospinal fluid (CSF) concentrations. (*A*), Kaplan-Meier survival curve. *B–F,* Viral RNA copy concentrations in whole blood (*B*), serum (*C*), CSF (*D*), oral swab (*E*), and nasal swab (*F*) samples. Viral RNA was detected in 4 of 6 animals, with no detectable viral RNA in oral (*E*) and nasal (*F*) mucosa in animal 8168, which succumbed on day 5 after exposure, or in 1 survivor (8212). The other survivor (8671) had peak viral replication in mucosa on day 9 after exposure, which then dropped to normal on day 12 after exposure.

signal intensity on trace (DT) maps (restricted diffusion). Both precontrast and postcontrast T1 values increased on the terminal day without contrast enhancement (data not shown).

In the second animal (8233), multiple lesions were seen on FLAIR and T2-weighted images on days 15 and then developed more on day 20 after exposure (Figure 3; brainstem lesion) in the pons and subcortical white matter of both cerebral hemispheres. All 5 hyperintense lesions showed facilitated diffusion to different degrees. The lesions showed increased signal intensity on T2-weighted, FLAIR, and DW images with increased trace (DT) values. Both precontrast (data not shown) and postcontrast T1 values increased on the terminal day (day 20 after exposure), with only 1 lesion in the right side of the midbrain showing subtle qualitative contrast enhancement. In the third animal (8112; not shown), only 1 focus of restricted diffusion was seen in the right internal capsule on days 12 and 15 after exposure.

In the survivor (animal 8671), 2 focal high signal intensity lesions were seen on FLAIR and T2-weighted images (data not shown) in the right frontal subcortical white matter and the left cerebellar white matter starting on day 12 after exposure (Figure 4). The former lesion was resolved on day 22, whereas the latter lesion decreased in size but remained detectable until the terminal day (day 56) (Figure 4). Both lesions showed increased diffusion on DW images, suggesting vasogenic edema. The overall brain volume remained unchanged during disease

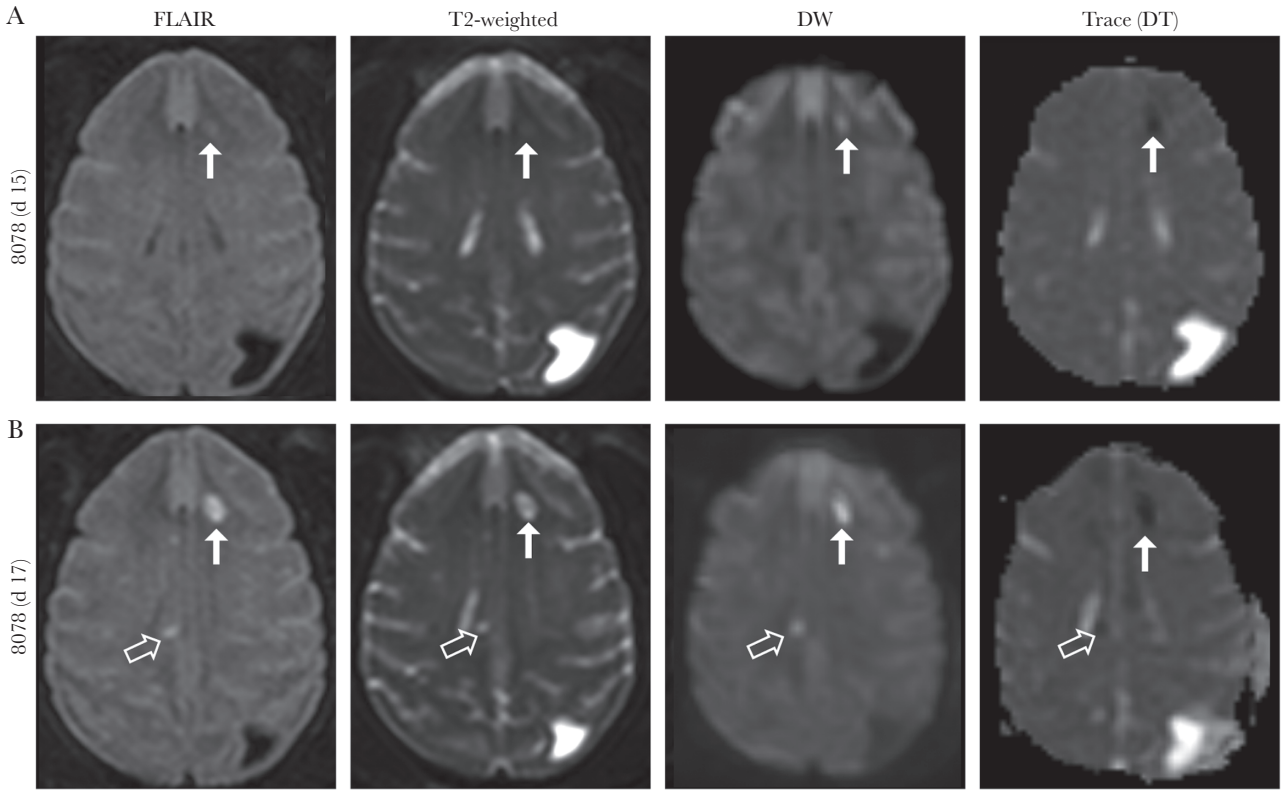

Figure 2. (*A*), A small focal lesion (arrows) appeared on day 15 after exposure in the left frontal subcortical white matter in 1 animal (8078). (*B*), Progression of disease is noted on day 17 (terminal day), with a total of 7 abnormal signal intensities now seen bilaterally. Incidental note is made of a preexisting congenital abnormality in this animal (colpocephaly, dilatation of the left posterior occipital horn). Abbreviations: DW, diffusion weighted; FLAIR, fluid-attenuated inversion-recovery; trace (DT), trace of diffusion tensor.

progression in all 6 animals (mean [standard deviation] coefficient of variation (CoV), 1.54 [0.63]).

Gross Pathology, Histology, and Histopathology

NiV-specific antibodies were noted in 3 of 6 animals, including 1 of the survivors (8671), whereas the other survivor (8212) did not mount an antibody response. Histopathology of the lesions with facilitated diffusion showed areas of encephalitis (Figure 5*A*) with perivascular CD3 (T-cell)–positive and CD68 (macrophage/monocyte)–positive infiltrates penetrating the surrounding parenchyma (Figure 5*C* and 5*D* with inset). Staining for microglia using the Iba1 marker identified foci of positive cells, whereas positive staining for glial cells using the GFAP marker was more widely positive. Weak neuronal nuclei (Figure 5*E*) and focal areas of positivity for cleaved caspase 3 (Figure 5*F* with inset) indicate areas of cellular apoptosis. Weak nonspecific NiV immunoreactivity was observed in these affected areas (not shown).

In areas of ischemia-related encephalomalacia, there was significant parenchymal loss (Figure 6*A*) with adjacent areas of nonsuppurative encephalitis with perivascular cuffing and vasculitis (Figure 6*A* inset) and specific NiV antigen staining of neurons (Figure 6*A* inset). In the adjacent areas of non-suppurative encephalitis, there is minimal Iba1 immunoreactivity (Figure 6*B*), and positive staining for GFAP was widely positive (not shown). There were significant focally extensive perivascular and parenchymal CD3 (T-cell)–positive infiltrates (Figure 6*C* with inset) and minimal CD68 (macrophage/monocyte)–positive infiltrates penetrating the surrounding parenchyma (Figure 6*D* with inset). Marked reduction of NeuN was observed in the region of encephalomalacia (Figure 6*E*). Additional focal areas of positivity for cleaved caspase 3 were also seen (Figure 6*F* with inset), indicating areas of cellular apoptosis.

DISCUSSION

The primary objective of this study was to use a large-particle, low-dose aerosol to develop a consistent neurological model for NiV infection that mimics a potential exposure route for humans. A secondary objective was to characterize the response to NiV through neuroimaging to understand pathogenicity in the AGM model that might and compare it to human disease of observed

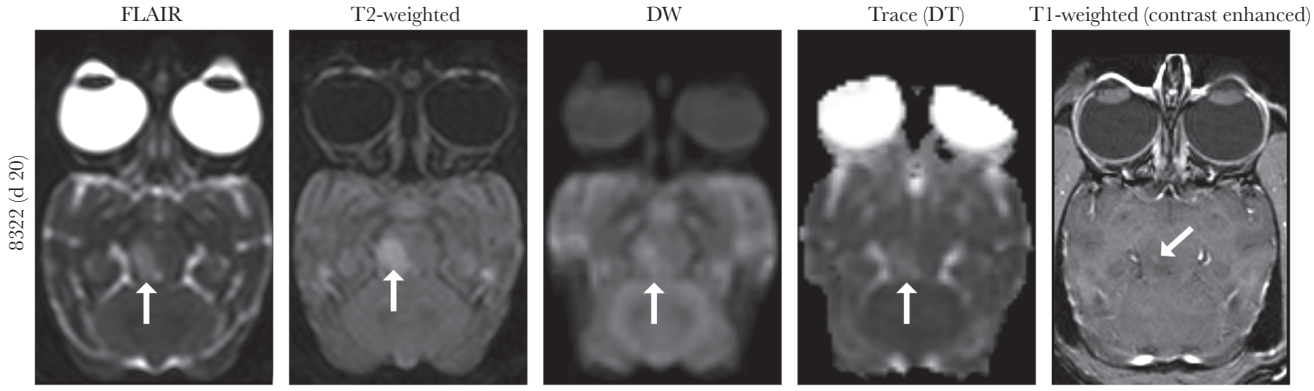

Figure 3. Magnetic resonance imaging of animal 8233 shows a focal lesion with increased T2-weighted and fluid-attenuated inversion-recovery (FLAIR) signal intensity on the right side of the midbrain on day 20 after exposure. This lesion demonstrated facilitated (non-restricted) diffusion (white arrows). Four other smaller lesions with similar characteristics were seen in this animal (not shown). Abbreviations: DW, diffusion weighted; trace (DT), trace of diffusion tensor.

in human NiV disease, which is a variant presentation of disease. The Malaysian isolate of NiV was used in this study to retain consistency with the initially described AGM model for NiV infection and with previously described work with intratracheal inoculation and small- to medium-particle aerosol exposure [21, 23, 25]. Some studies suggest that the Malaysian isolate of NiV has been associated with neurological disease whereas the Bangladesh isolate of NiV may be more closely aligned to development of respiratory disease in humans [35, 36]. However, our group showed prominent respiratory features and rapidly progressing disease after NiV infection with NiV-M strain [23, 25].

In the current study, we found that exposure to the large-particle aerosol and a lower virus dose led to an extended disease course and neurological disease in all animals with clinical evidence of infection. Brain MR imaging identified lesions and structural changes in the brains of 4 animals, including 1 survivor, changes that were similar to previously reported abnormalities in NiV-infected patients in Singapore and Malaysia [14–16, 37]. Another surviving animal had no lesions or structural brain changes but also showed no evidence of being infected. It is still unclear how 1 animal was not apparently infected despite known exposure. However, this finding emphasizes the biological diversity that exists in outbred animals and also reflects the variable disease course seen in humans.

Our findings suggest 2 major pathologies in the brain on exposure to NiV. The first finding includes small ischemic foci indicated by lesions with restricted diffusion that probably reflect vasculitis and secondary vascular occlusion, mediated by NiV involvement of the endothelial cells. This finding was described previously in infected patients and was generally assumed to reflect vasculitis [3, 15, 16]. In 1 of these reports, systemic vasculitis was shown with endothelial damage and syncytial cell formation [3]. The locations of these reported lesions in general were similar to those we observed in our animals. On histological examination, we saw areas of encephalomalacia corresponding to the foci of ischemia because the brains were sampled well after the original ischemic events. At that point, acute inflammatory changes were expected to have resolved,

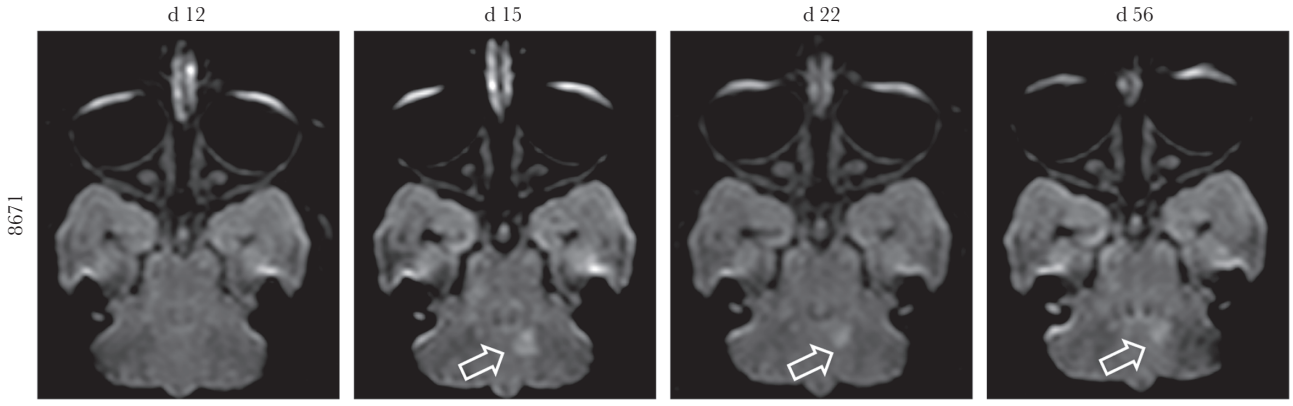

Figure 4. Longitudinal changes on fluid-attenuated inversion-recovery images in a survivor (8671). Focal area of increased signal in the left cerebellar hemisphere (arrows) appeared on day 15 after exposure and decreased in size over time. The lesion was still noted, but to a lesser extent, on day 56 after exposure, the study end point.

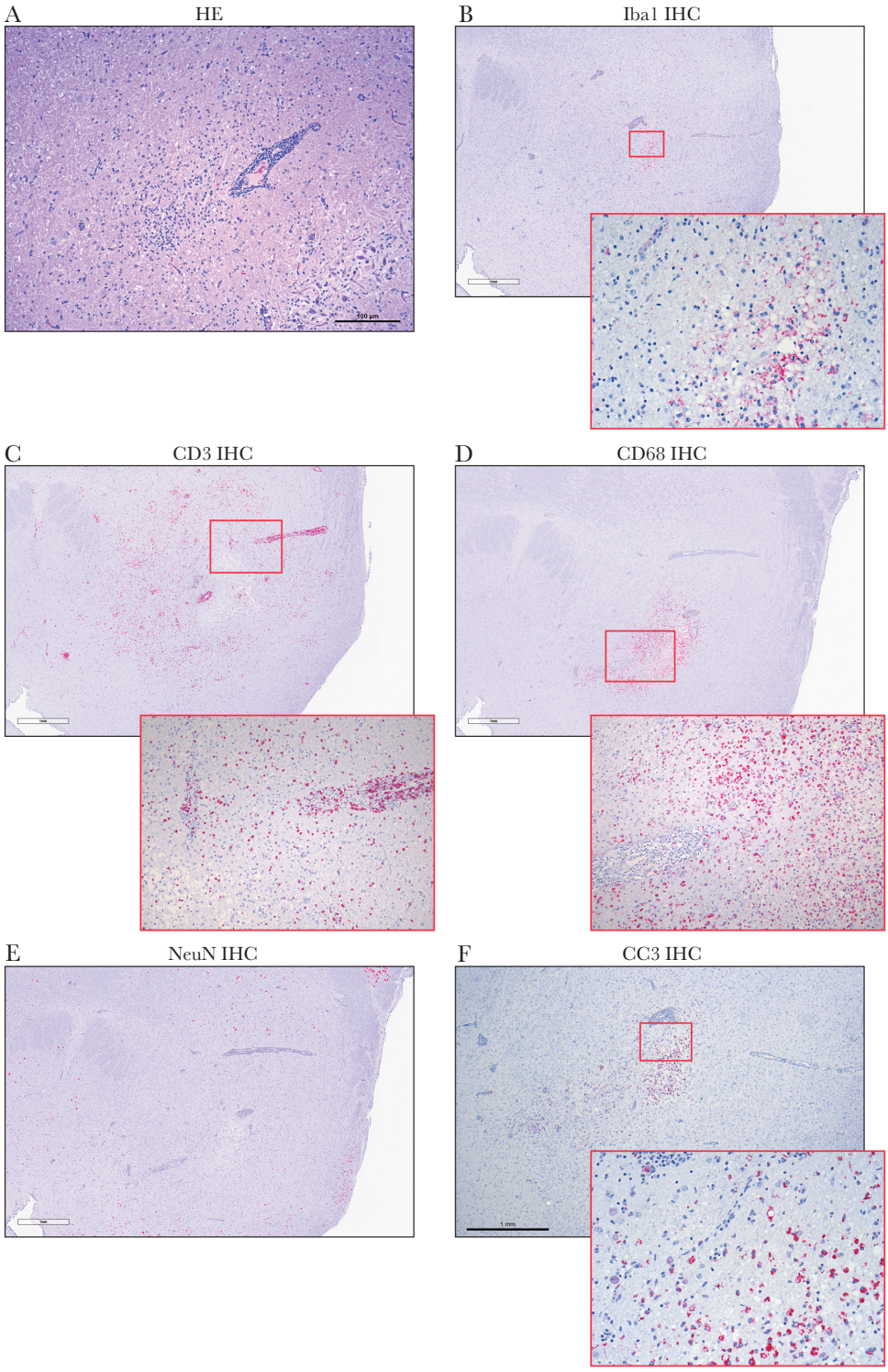

Figure 5. Histopathological findings showing encephalitis (8233). (*A*), Hematoxylin-eosin (HE) staining of brain with perivascular infiltrates of inflammatory cells extending into surrounding parenchyma. (*B–F*), Immunohistochemistry (IHC) signal changes, (*B*), Focal ionized calcium-binding adaptor molecule 1 (Iba1) IHC signal indicating microglial response (inset; original magnification ×200). (*C*), Perivascular CD3-positive T-cell infiltrates, extending into surrounding parenchyma (inset; original magnification ×200). (*D*), CD68 positive monocyte/macrophage infiltrates penetrating the surrounding parenchyma in conjunction with T-cell infiltrates (inset; original magnification ×200). (*E*), Locally absent neuronal nuclei (NeuN) IHC signal. (*F*), Focal extensive areas of positivity for cleaved caspase 3 (CC3) (inset; original magnification ×200) indicate areas with cellular apoptosis.

and gliosis or encephalomalacia would appear instead. This expectation is consistent with negative staining for NiV antigen and with infiltrating T cells and macrophages.

The second pathological finding we observed was more consistent with encephalitis: increased diffusion on MR imaging, indicating vasogenic edema. Those encephalitic foci showed

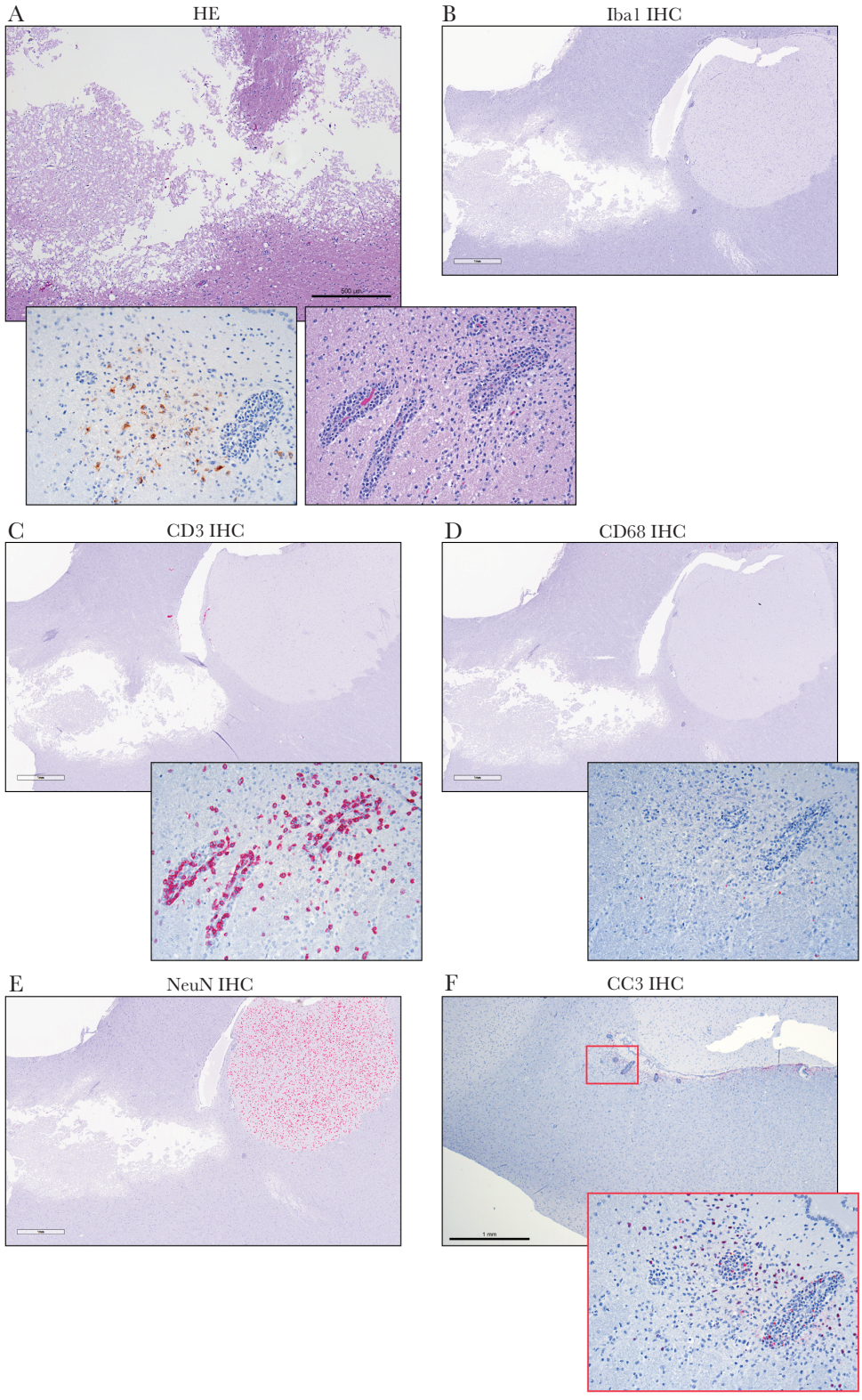

Figure 6. Ischemia-related encephalomalacia within the frontal lobe of animal 8078. (*A*), Large area of encephalomalacia with parenchymal loss with adjacent, nonsuppurative encephalitis (inset; original magnification ×200). Left inset shows specific NiV antigen staining of neurons; right inset, perivascular inflammatory infiltrates and vasculitis. (*B–F*), Immunohistochemistry (IHC) signal changes. (*B*), No significant ionized calcium-binding adaptor molecule 1 (Iba1) IHC signal. (*C*), Perivascular CD3 positive T-cell infiltrates, extending into surrounding parenchyma (inset; original magnification ×200). (*D*), Minimal CD68 positive monocyte/macrophage infiltrates (inset; original magnification ×200). (*E*), locally absent neuronal nuclei (NeuN) IHC signal in the area of the lesion, strongly present in areas not affected. (*F*), focal extensive areas of positivity for cleaved caspase (CC3) (inset; original magnification ×200) indicate areas with cellular apoptosis. Abbreviation: HE, hematoxylin-eosin.

typical microglial/macrophage activation, with T-cell and macrophage infiltration along with neuronal loss. Interestingly, those lesions were located mostly in the posterior fossa, involving the cerebellum or the brainstem, similar to lesions reported by Lim et al [15]. We noticed subtle enhancement in 1 of those lesions, similar to previously reported enhancement [15], consistent with a disrupted blood-brain barrier.

What determines the nature of brain involvement in the AGM model is unclear; however, the presence of ischemic lesions seems to point toward more severe disease. In 2 animals with restricted diffusion lesions, the CSF was positive for viral RNA. In contrast, the other animals, including the survivor with non-restricted diffusion lesions, did not have NiV RNA in the CSF. Because this model was not uniformly lethal, and because recurrence of NiV disease is relatively common, future studies should involve monitoring surviving animals long term with MR imaging and clinical observation to look for recurrent NiV encephalitis and help elucidate that phenomenon.

In conclusion, we have developed an animal model of NiV infection that closely reproduces the central nervous system disease previously described in infected humans. This model opens the door for better understanding of the nature of NiV involvement in the brain. The availability of MR imaging in a BSL-4 environment also provides us with a great opportunity to identify the presence of brain involvement in vivo, in real time as well as potential reversal of disease under the effect of therapeutic or preventive strategies. These results, combined with a further study of immune responses, may explain why certain animals did not get infected. The end goal would be to develop strategies that prevent or curb central nervous system involvement with NiV in infected patients to avoid long-lasting damage associated with various degrees of vasculitis or ischemia and/or viral encephalitic changes.

Supplementary Data

Supplementary materials are available at *The Journal of Infectious Diseases* online. Consisting of data provided by the authors to benefit the reader, the posted materials are not copyedited and are the sole responsibility of the authors, so questions or comments should be addressed to the corresponding author.

Notes

Acknowledgments. We thank the comparative medicine, clinical services, histology and imaging teams at the Integrated Research Facility, without whose effort this work could not be completed. We also thank Timothy Cooper, DVM, PhD, who performed several necropsies, Irwin Feuerstein, MD, who reviewed radiological images, and Jiro Wada for his efforts with figure preparation; all 3 are from the Integrated Research Facility.

Disclaimer. The content of this publication does not necessarily reflect the views or policies of the Department of Health and Human Services, nor does mention of trade names, commercial products, or organizations imply endorsement by the US government.

Financial support. This work was supported by the Division of Intramural Research and the Division of Clinical Research, National Institute of Allergy and Infectious Diseases and was performed under a Battelle Memorial Institute contract with the National Institute of Allergy and Infectious Diseases (contract HHSN272200700016I). Additional support was provided by the National Cancer Institute (contract HHSN261200800001E).

Potential conflicts of interest. All authors: no reported conflicts. All authors have submitted the ICMJE Form for Disclosure of Potential Conflicts of Interest. Conflicts that the editors consider relevant to the content of the manuscript have been disclosed.

References

1. Chua KB, Bellini WJ, Rota PA, et al. Nipah virus: a recently emergent deadly paramyxovirus. Science **2000**; 288:1432–5.
2. Centers for Disease Control and Prevention. Outbreak of Hendra-like virus—Malaysia and Singapore, 1998–1999. MMWR Morb Mortal Wkly Rep **1999**; 48:265–9.
3. Paton NI, Leo YS, Zaki SR, et al. Outbreak of Nipah virus infection among abattoir workers in Singapore. Lancet **1999**; 354:1253–6.
4. Sahani M, Parashar UD, Ali R, et al. Nipah virus infection among abattoir workers in Malaysia, 1998–1999. Int J Epidemiol **2001**; 30:1017–20.
5. World Health Organization Regional Office for South-East Asia. Nipah virus outbreaks in the WHO South-East Asia region. http://www.searo.who.int/entity/emerging_diseases/links/nipah_virus_outbreaks_sear/en/. Accessed 14 June 2019.
6. Chadha MS, Comer JA, Lowe L, et al. Nipah virus-associated encephalitis outbreak, Siliguri, India. Emerg Infect Dis **2006**; 12:235–40.
7. Tan CT, Tan KS. Nosocomial transmissibility of Nipah virus. J Infect Dis **2001**; 184:1367.
8. Hossain MJ, Gurley ES, Montgomery JM, et al. Clinical presentation of Nipah virus infection in Bangladesh. Clin Infect Dis **2008**; 46:977–84.
9. Mathieu C, Horvat B. Henipavirus pathogenesis and antiviral approaches. Expert Rev Anti Infect Ther **2015**; 13:343–54.
10. Sherrini BA, Chong TT. Nipah encephalitis—an update. Med J Malaysia **2014**; 69(suppl A):103–11.
11. Abdullah S, Tan CT. Henipavirus encephalitis. Handb Clin Neurol **2014**; 123:663–70.
12. Ng BY, Lim CC, Yeoh A, Lee WL. Neuropsychiatric sequelae of Nipah virus encephalitis. J Neuropsychiatry Clin Neurosci **2004**; 16:500–4.
13. Sejvar JJ, Hossain J, Saha SK, et al. Long-term neurological and functional outcome in Nipah virus infection. Ann Neurol **2007**; 62:235–42.

14. Goh KJ, Tan CT, Chew NK, et al. Clinical features of Nipah virus encephalitis among pig farmers in Malaysia. N Engl J Med **2000**; 342:1229–35.
15. Lim CC, Sitoh YY, Hui F, et al. Nipah viral encephalitis or Japanese encephalitis? MR findings in a new zoonotic disease. AJNR Am J Neuroradiol **2000**; 21:455–61.
16. Sarji SA, Abdullah BJ, Goh KJ, Tan CT, Wong KT. MR imaging features of Nipah encephalitis. AJR Am J Roentgenol **2000**; 175:437–42.
17. Engeler CE, Tashjian JH, Trenkner SW, Walsh JW. Ground-glass opacity of the lung parenchyma: a guide to analysis with high-resolution CT. AJR Am J Roentgenol **1993**; 160:249–51.
18. Institute of Epidemiology Disease Control and Research. Nipah cases and death report. https://www.iedcr.gov.bd/index.php/surveillance/212-nipahreport. Accessed 17 July 2019.
19. Dabisch PA, Xu Z, Boydston JA, et al. Quantification of regional aerosol deposition patterns as a function of aerodynamic particle size in rhesus macaques using PET/CT imaging. Inhal Toxicol **2017**; 29:506–15.
20. Geisbert TW, Daddario-DiCaprio KM, Hickey AC, et al. Development of an acute and highly pathogenic nonhuman primate model of Nipah virus infection. PLoS One **2010**; 5:e10690.
21. Johnston SC, Briese T, Bell TM, et al. Detailed analysis of the African green monkey model of Nipah virus disease. PLoS One **2015**; 10:e0117817.
22. Mire CE, Satterfield BA, Geisbert JB, et al. Pathogenic differences between Nipah virus Bangladesh and Malaysia strains in primates: implications for antibody therapy. Sci Rep **2016**; 6:30916.
23. Cong Y, Lentz MR, Lara A, et al. Loss in lung volume and changes in the immune response demonstrate disease progression in African green monkeys infected by small-particle aerosol and intratracheal exposure to Nipah virus. PLoS Negl Trop Dis **2017**; 11:e0005532.
24. Yoneda M, Georges-Courbot MC, Ikeda F, et al. Recombinant measles virus vaccine expressing the Nipah virus glycoprotein protects against lethal Nipah virus challenge. PLoS One **2013**; 8:e58414.
25. Hammoud DA, Lentz MR, Lara A, et al. Aerosol exposure to intermediate size Nipah virus particles induces neurological disease in African green monkeys. PLoS Negl Trop Dis **2018**; 12:e0006978.
26. Guide for the Care and Use of Laboratory Animals. 8th Ed. Washington, DC: National Academies Press. https://grants.nih.gov/grants/olaw/guide-for-the-care-and-use-of-laboratory-animals.pdf
27. Hartings JM, Roy CJ. The automated bioaerosol exposure system: preclinical platform development and a respiratory dosimetry application with nonhuman primates. J Pharmacol Toxicol Methods **2004**; 49:39–55.
28. Jensen KS, Adams R, Bennett RS, Bernbaum J, Jahrling PB, Holbrook MR. Development of a novel real-time polymerase chain reaction assay for the quantitative detection of Nipah virus replicative viral RNA. PLoS One **2018**; 13:e0199534.
29. Castro MA, Yao J, Pang Y, et al. Template-based B_1 inhomogeneity correction in 3T MRI brain studies. IEEE Trans Med Imaging **2010**; 29:1927–41.
30. Irfanoglu MO, Modi P, Nayak A, Hutchinson EB, Sarlls J, Pierpaoli C. DR-BUDDI (Diffeomorphic Registration for Blip-Up blip-Down Diffusion Imaging) method for correcting echo planar imaging distortions. Neuroimage **2015**; 106:284–99.
31. Pierpaoli C, Walker L, Irfanoglu MO, et al. TORTOISE: an integrated software package for processing of diffusion MRI data. In: International Society for Magnetic Resonance in Medicine 18th annual meeting. Stockholm, Sweden: International Society for Magnetic Resonance in Medicine, **2010**:1597.
32. Irfanoglu MO, Modi P, Nayak A, Knutsen A, Sarlls J, Pierpaoli C. DR-BUDDI: diffeomorphic registration for blip up-down diffusion imaging. Med Image Comput Comput Assist Interv **2014**; 17:218–26.
33. Reveley C, Gruslys A, Ye FQ, et al. Three-dimensional digital template atlas of the macaque brain. Cereb Cortex **2017**; 27:4463–77.
34. Liddie S, Goody RJ, Valles R, Lawrence MS. Clinical chemistry and hematology values in a Caribbean population of African green monkeys. J Med Primatol **2010**; 39:389–98.
35. Nikolay B, Salje H, Hossain MJ, et al. Transmission of Nipah virus—14 years of investigations in Bangladesh. N Engl J Med **2019**; 380:1804–14.
36. Chua KB, Lam SK, Goh KJ, et al. The presence of Nipah virus in respiratory secretions and urine of patients during an outbreak of Nipah virus encephalitis in Malaysia. J Infect **2001**; 42:40–3.
37. Lam SK, Chua KB. Nipah virus encephalitis outbreak in Malaysia. Clin Infect Dis **2002**; 34(suppl 2):S48–51.